Investigating the physiology behind nose thermal response to stress: a cross-mapping approach

Federica Gioia[1], Mimma Nardelli[1,2], Enzo Pasquale Scilingo[1,2], and Alberto Greco[1,2]

[1] Deparment of Information Engineering, University of Pisa, Pisa, Italy
[2] Research Center "E. Piaggio", University of Pisa, Pisa, Italy
federica.gioia@phd.unipi.it

Abstract. InfraRed Thermography (IRT) is an innovative monitoring tool, very beneficial in the field of psychophysiology to assess mental states in a completely non-invasive manner. IRT is contactless and it measures the temperature of the skin remotely. Thermal patterns of the skin are driven by the autonomic nervous system, thus, they reflect autonomic responses to affective stimuli. Insights into the physiology behind changes in facial thermal patterns could improve our thermography-based inferences reaching greater emotional specificity.
Here, we used a cross-mapping approach to investigate the nonlinear correlations between IRT and heart rate variability (HRV), which is a powerful tool for characterizing cardiovascular activity. We used thermal signals of the nose and HRV data from 30 subjects during a resting state and under a stressful stimulation task. Our results show a statistically significant nonlinear correlation between the time series, with a significant increase in the correlation values during the stressor.
Our preliminary results give a foundation to the hypothesis that the stress-induced decrease in the nose temperature is related to sympathetic-induced vasomotor activity.

Keywords: thermal imaging, nose, heart rate variability, cross-mapping

1 Introduction

In the last decades, infrared thermography (IRT) has captured the attention of researchers in the psychophysiological field, amongst many others. Facial thermal variations have been associated with the autonomic nervous system (ANS) activity, hence allowing inferences of affective nature [1]. The ANS regulates the visceral responses, modulating the activity of its two branches, the sympathetic (SNS) and the parasympathetic systems (PNS). Many studies have explored the degree of autonomic emotion specificity, analyzing the different patterns in peripheral physiological responses to a variety of affective stimuli [2–4]. Compared to other physiological measures, this cutting-edge technology has the great advantage of being a contactless non-invasive diagnostic and monitoring tool. In fact, IRT measures the temperature of the skin of the subjects at a distance, by detecting the IR energy that any body, at a temperature higher than absolute zero, emits.

IRT has been proven to be reliable and efficient for stress monitoring in several studies [1, 5–12]. To this aim, the most relevant region of interest is the tip of the nose. The temperature of the nose decreases during stressful situations and increases due to an empathetic response [1, 10–12]. The hypothesis is that the ANS influences the vasomotor activity of the subcutaneous vessels and consequently the dynamics of the blood circulation which produces the temperature variation [12–14]. However, this is not the only process involved in temperature regulation, also sweating, respiration and metabolic processes play a crucial role [1, 12, 15]. It is now common knowledge that physiological processes have nonlinear dynamics [16]. In particular, specific aspects of the activity of human thermoregulatory system can show nonlinear dynamics that have been compared to the behaviour of theoretical nonlinear systems [17, 18].

This study aims to provide insights into the ANS correlates of nose temperature modulation in response to emotional stimuli. We want to give a foundation to the hypotheses that have prevailed in the interpretation of the results obtained in thermography studies applied to the recognition of the emotional state. Specifically, we focused on the link between the thermal signal of the nose with the heart rate variability (HRV) signal, which is a powerful tool for characterizing cardiovascular activity [19]. We used a cross-mapping approach to quantify the nonlinear correlations between IRT and HRV dynamics [20–22]. Particularly, we applied this analysis to thermal signals extracted from the nose region and to HRV time series recorded from healthy subjects during rest and under a stressful stimulus, to address the question both under parasympathetic and sympathetic nervous system predominance conditions, respectively.

2 Materials and Methods

2.1 Subjects recruitment and experimental set-up

Thirty healthy volunteers (20 females, age = 26.6 ± 3.6) participated in the study. None of them had any history of mental disorders or cardiovascular diseases. Coffee and smoke were forbidden on the same day of the experiment to avoid the potential vasomotor effects of these substances. The experiments were conducted in a controlled environment. In particular, the room environmental conditions were kept constant and at comfortable levels of temperature and humidity, around 24-26°C and 40-60%, respectively. All recordings took place away from direct heat and ventilation sources. Subjects were asked to sit in a comfortable chair in the experimental room for at least 10 minutes before the acquisition started. This acclimatization period limited the thermoregulation processes during the acquisition. This experiment was approved by the "Bioethics Committee of the University of Pisa" (n. 15/2019), and each subject signed the informed consent upon arrival.

The experiment comprised two main phases: a resting session and a stress stimulation, lasting 5 minutes each. We developed a Psychopy application adhoc for this experiment. The application ran on a laptop and guided the subject throughout the experimental phases. The protocol timeline is shown in Figure 1. Before and after the experiment, each subject completed the State-Trait Anxiety Inventory (STAY-Y1), a psychometric test consisting of 20 self-report items on a 4-point Likert scale to measure state anxiety. Moreover, the subject was required to report its self-assessed perceived stress (PS) level on a Likert scale from 0 (not at all) to 10 (very stressed), before and after the stressor. During the resting session, the subjects were asked to stare at a fixation cross in the middle of the screen. During the stimulation phase, stress was induced using a computerized and paced Stroop test [23]. In particular, the subject was required to solve incongruous color/semantic-meaning stimuli every 2 seconds. In addition, at the top of the screen, a counter kept track of the number of consecutive successes, as a motivational stressor.

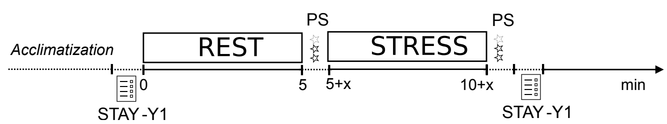

Fig. 1. Protocol timeline. The dashed line indicates non-timed tasks.

We acquired the thermograms of the face of the subjects using a FLIR T640 thermal camera with a 24.6mm lens, 640x480 pixels, NETD < 0.04mK @ $+30°$ and spectral range of 7.8-14 μm (Long-wave-infrared, LWIR). The sampling frequency was 5 Hz. In addition, RGB images in the visible spectrum were recorded using a Logitech HD WebCam C270. The two cameras, IR and RGB, were vertically aligned. Each subject was asked to find a comfortable position and stay still during the recordings, using a chin rest to avoid any movement artifacts. Moreover, we acquired the electrocardiogram (ECG) using a BIOPAC MP150 system, at a sampling rate of 250Hz. Three Ag/AgCl electrodes were placed below the right and left clavicle, and on the lower left chest to measure the ECG signal.

2.2 ECG and thermal time series processing

Both ECG and thermal time series were segmented into 150-second-long segments for each experimental session (i.e., rest and stress sessions). In particular, we selected the last half of the resting session as a baseline, to make sure subjects had completely recovered from the distress caused by the setup process. Conversely, only the first half of the stress session was used for the analysis to maximize the stressful effect and mitigate the habituation effect on the stimulation phase. Hereinafter, we will refer to these segments as *Rest* and *Stress*, respectively.

The thermal time series of the tip of the nose was extracted from the thermograms. We used the RGB images to localize the region of interest (ROI), and we referred the RGB coordinates to the IR frames to obtain the thermal information. To this aim, we synchronized and registered the first IR and RGB frames. In particular, we selected the first frame of the RGB series and applied an affine-2D transformation to match the corresponding IR frame. Then, the coordinates of the centre of the ROI were automatically detected by applying the Yuval Nirkin algorithm on the registered RGB frame [24]. Furthermore, we segmented each subject's face using a landmark-intensity-based algorithm, as explained in [25]. Thus, the number of pixels of the face of the subject was used to choose the dimension of the ROI, accounting for the inter-subjects differences in face shapes and sizes. Finally, the thermal signal was obtained as the median temperature within the ROI for each thermogram. For each of the two sessions, we calculated the mean of the thermal signal of the nose.

Concerning the ECG signals, the signals were pre-processed using the Kubios software to remove noise and artifacts and extract the Heart Rate Variability (HRV) series [26]. Specifically, interbeat interval series (RR series) were extracted from ECG signals using the Pan-Tompkins algorithm to automatically detect the QRS complexes. Then, the HRV series were extracted by interpolating the RR series through a piecewise cubic interpolation at 5 Hz. From the HRV segments related to both the *Rest* and *Stress* sessions, we extracted some of the standard features belonging to time and frequency domains, as reported in Table 1.

Of note, two female subjects were excluded from the analysis due to the presence of irreducible artifacts.

Table 1. Features extracted from the HRV

Feature	**Description**
meanHRV	Mean value of HRV
stdHRV	Standard deviation of HRV
RMSSD	Root mean square of successive RR interval differences
pNN50	Percentage of successive RR intervals that differ by more than 50ms
LF	Percentage of the total power in the low-frequency (0.04–0.15 Hz)
HF	Percentage of the total power in the low-frequency (0.15–0.40 Hz)
LF/HF ratio	Ratio of LF to HF power

2.3 Cross-mapping

The cross-mapping procedure [20, 21] was applied to compute an estimate of the IR time series (Y = (Y_1, Y_2, ..., Y_n)) from the HRV one (X = (X_1, X_2, ..., X_n)). We can use the delayed version of one time series to reconstruct a shadow manifold, which is an approximation to the true attractor of the dynamical system to which the series belongs. According to Takens' theorem, if X and Y are variables of the same dynamical system, the reconstructed attractors M_X and

M_Y are diffeomorphic to each other, as well as to the true attractor. In fact, if the two series represent a dimension in the state space, the knowledge of the shadow manifold M_X, obtained from the variable X, can be used to estimate variable Y. Hence, we observed the similarity between the time series $\hat{Y}$, estimated from variable X, and the original time series Y, to quantify the imprint of variable X on variable Y.

For each time series, we calculated the appropriate time delay τ as the minimum of the mutual information function, to ensure statistical independence between the values, in both linear and nonlinear terms. Moreover, we estimated the embedding dimension m, using the false nearest neighbour (FNN) method, as in [27]. Using time-delayed embedding, from each variable X and Y we constructed the shadow manifolds, M_X and M_Y.

Afterwards, we identified the m+1 nearest-neighbours in M_X over time. The number of neighbours depends on the maximum value of embedding dimension m between the two time series. The time index of these m+1 points in M_X was used to obtain the corresponding points in M_Y. These points in M_Y were used to map a region of m+1 points around Y_t. Finally, the estimate of each point of Y starting from the reconstructed manifold of X is found as follows:

$$\hat{Y}_t|M_X = \sum_{i=1}^{m+1} \omega_i Y_{t_i}$$

Where ω_i are the weights obtained as the Euclidean distances between X_t and the nearest-neighbours points ($||\cdot||$ indicates the Euclidean distance in $\mathbb{R}^m$):

$$\omega_i = \frac{u_i}{\sum_{j=1}^{m+1} u_j}$$

$$u_i = exp\left[-\frac{||X_t - X_{t_i}||}{||X_t - X_{t_1}||}\right]$$

Finally, we computed the Pearson correlation coefficient between the original thermal signals and the corresponding estimates obtained using cross-mapping, and we will refer to it as $\rho_{\hat{Y}Y}$. Similarly, we computed the Pearson correlation coefficients between the original thermal signals and the HRV time series, ρ_{XY}.

2.4 Statistical analysis

We performed an exploratory statistical analysis to evaluate the effect of the stress stimulus on the psychometric scores and the IR and cardiovascular dynamics. We used the non-parametric Wilcoxon sign-rank test to compare the STAY-Y1 and PS scores before and after the stressor. Analogously, we used the same test to compare each IR and HRV feature between *Rest* and *Stress* (α = 0.05). We controlled for the false discovery rate that results from multiple testing through the Benjamini, Krieger, and Yekutieli (FDR-BKY) correction [28].

In addition, we assessed the significance level of each correlation coefficient $\rho_{\hat{Y}Y}$ using a non-parametric permutation test with 1000 repetitions ($\alpha = 0.05$).

The original thermal signal was divided into blocks of length equal to τ, which were randomly shuffled at each iteration to generate the null distribution. In this way, maximizing independence among blocks, we mitigate the effect of autocorrelation in the time series in causing spurious correlations between variables. Likewise, we assessed the significance levels of the Pearson correlation coefficients ρ_{XY} using the same permutation test.

Finally, a non-parametric Wilcoxon sign-rank test was used to test for possible differences between the correlation coefficient $\rho_{\hat{Y}Y}$ related to the *Rest* and *Stress* sessions. Of note, the use of non-parametric statistical tests was justified by the non-gaussian distributions of samples.

3 Results

The statistical analysis on both psychometric tests indicated that subjects reported to be more stressed after the stimulation. In particular, the Wilcoxon sign-rank test on the PS levels reported a p-value equal to 0.01, and the p-value for the STAY-Y1 total scores was equal to 0.03.

Regarding the physiological features, the mean temperature of the nose decreased significantly during *Stress* compared to *Rest*. Conversely, the mean of HRV increased significantly during *Stress*. The remaining HRV features, except the *LF/HF ratio*, decreased significantly compared to *Rest*, as shown in Figure 2.

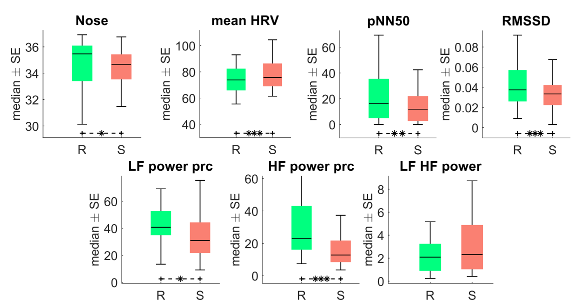

Fig. 2. Statistical comparison for each of the IR and HRV features extracted. Significant differences between *Rest* = R and *Stress* = S after the Wilcoxon signed rank test with FDR-BKY correction are highlighted with an asterisk (* = $p < 0.05$; ** = $p < 0.01$; ***= $p < 0.001$).

The results of the correlation between the original thermal signals and the HRV series ρ_{XY}, and the correlation between the original thermal signals and their reconstructed version from the HRV time series $\rho_{\hat{Y}Y}$, are shown in Table 2. In particular, the median of the correlation coefficients ρ_{XY} was 0.005 during *Rest*, and it was statistically significant in 17.86% of the subjects. During *Stress*, the median of the correlation coefficients ρ_{XY} was equal to -0.123, and it was statistically significant in 60.71% of the subjects. The median of the $\rho_{\hat{Y}Y}$ was equal to 0.7 during *Rest* and it increased to 0.78 during *Stress*. Note that, the associated p-values were significant for all the subjects (100%).

Table 2. Non-parametric permutation test on correlation coefficient values ρ_{XY} and $\rho_{\hat{Y}Y}$.

	Rest		Stress	
	ρ median	p-val<0.05 (%)	ρ median	p-val<0.05 (%)
ρ_{XY}	0.005	17.86	-0.123	60.71
$\rho_{\hat{Y}Y}$	0.7	100	0.78	100

The boxplots in Figure 3 show the values of the correlation coefficient $\rho_{\hat{Y}Y}$ obtained after the application of the cross-mapping approach to the thermal signals of the nose and the HRV time series. After the Wilcoxon signed rank test, the $\rho_{\hat{Y}Y}$ values were significantly higher during *Stress* than *Rest*.

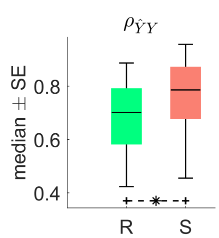

Fig. 3. Statistical comparison of $\rho_{\hat{Y}Y}$ coefficient values obtained after the application of cross-mapping method on thermal and HRV data, between *Rest* = R and *Stress* = S. Significant differences after the Wilcoxon signed rank test are highlighted with an asterisk (* = $p < 0.05$).

4 Discussions and Conclusions

An understanding of the physiological processes driving changes in the facial temperature pattern could improve our thermography-based inferences in the field of psychophysiology. Greater emotional specificity would broaden the scope of IRT as a convenient non-contact method for monitoring changes in mental state. Although there are already hypotheses on the mechanisms that influence skin temperature, the quantification of these processes and their interplay is still lacking. This study reports an attempt to investigate the linear and non-linear relation between the thermal behaviour of the nose and cardiovascular activity, under both parasympathetic and sympathetic dominance. We used the cross-mapping approach [20, 21], a nonlinear methodology based on chaos theory to quantify the agreement between HRV and nose thermal time series.

Prior to the cross-mapping analysis, we tested the difference in the psychometric scores reported before and after the stimulation. Similarly, we performed a comparison of thermal and HRV features between the two experimental sessions. The results confirmed that the protocol elicited the expected response, as the reported stress level increased and the physiological features varied significantly in agreement with the literature. Notably, nose temperature decrease during stress has been previously associated with sympathetic vasoconstriction of the subcutaneous vessels. The RMSSD and the PNN50 are temporal indexes of the vagal activity, as the HF power in the frequency domain. Their decrease is likely to reflect a decrease in the PNS activity during stress.

Nonlinear analysis of the IR and HRV time series revealed a strong relation between the thermal and cardiovascular dynamics that was not obvious in the linear domain. Indeed, the linear correlation between the original HRV and thermal series was significant in the majority of the subjects during *Stress*. However, the correlation values ρ_{XY} reported a median value as low as 0.005. On the other hand, the correlation values between the thermal signals of the nose and their estimated version obtained using the cross-mapping approach with the HRV time series were significant for all the subjects during both *Rest* and *Stress*, with a median value higher than 0.7. This nonlinear correlation values quantify how the knowledge of the shadow manifold obtained from the time series of the HRV time series can be used to estimate values of the IR time series. Hence, we used the correlation value $\rho_{\hat{Y}Y}$ as an index of the 'imprint' of the HRV time series on the thermal signal of the nose.

Furthermore, the cross-mapping correlation values $\rho_{\hat{Y}Y}$ were significantly higher during *Stress* compared to *Rest*. This outcome suggests that cardiovascular activity and nose temperature coupling are higher during elevated arousal conditions. Hence, our approach seems to corroborate the hypothesis that the stress-induced decrease in the nose temperature is related to sympathetic-induced vasomotor activity [12–14].

In our future studies, we will analyze the linear and nonlinear correlations between thermal signals from different regions of the face and several physiological signals related to the phenomena which are likely to underlie skin temperature modulation (i.e. heart rate variability, electrodermal and respiratory activity).

References

1. Ioannou, S., Gallese, V. & Merla, A. Thermal infrared imaging in psychophysiology: potentialities and limits. *Psychophysiology* **51,** 951–963 (2014).
2. Cacioppo, J. T., Berntson, G. G., Klein, D. J. & Poehlmann, K. M. Psychophysiology of emotion across the life span. *Annual review of gerontology and geriatrics* **17,** 27–74 (1997).

3. Ekman, P. *et al.* Universals and cultural differences in the judgments of facial expressions of emotion. *Journal of personality and social psychology* **53,** 712 (1987).
4. Jerritta, S., Murugappan, M., Nagarajan, R. & Wan, K. *Physiological signals based human emotion recognition: a review* in *2011 IEEE 7th international colloquium on signal processing and its applications* (2011), 410–415.
5. Puri, C., Olson, L., Pavlidis, I., Levine, J. & Starren, J. *StressCam: noncontact measurement of users' emotional states through thermal imaging* in *CHI'05 extended abstracts on Human factors in computing systems* (2005), 1725–1728.
6. Cardone, D. *et al.* Driver stress state evaluation by means of thermal imaging: A supervised machine learning approach based on ECG signal. *Applied Sciences* **10,** 5673 (2020).
7. Perpetuini, D. *et al. Can Functional Infrared Thermal Imaging Estimate Mental Workload in Drivers as Evaluated by Sample Entropy of the fNIRS Signal?* in *8th European Medical and Biological Engineering Conference: Proceedings of the EMBEC 2020, November 29–December 3, 2020 Portorož, Slovenia* (2021), 223–232.
8. Němcová, A. *et al.* Multimodal Features for Detection of Driver Stress and Fatigue: Review. *IEEE Transactions on Intelligent Transportation Systems* **22,** 3214–3233 (2021).
9. Akbar, F. *et al. Email makes you sweat: Examining email interruptions and stress using thermal imaging* in *Proceedings of the 2019 CHI Conference on Human Factors in Computing Systems* (2019), 1–14.
10. Cho, Y., Bianchi-Berthouze, N., Oliveira, M., Holloway, C. & Julier, S. *Nose heat: Exploring stress-induced nasal thermal variability through mobile thermal imaging* in *2019 8th International Conference on Affective Computing and Intelligent Interaction (ACII)* (2019), 566–572.
11. Filippini, C., Spadolini, E., Cardone, D. & Merla, A. Thermal imaging based affective computing for educational robot. *Multidisciplinary Digital Publishing Institute Proceedings* **27,** 27 (2019).
12. Cho, Y., Julier, S. J. & Bianchi-Berthouze, N. Instant stress: detection of perceived mental stress through smartphone photoplethysmography and thermal imaging. *JMIR mental health* **6,** e10140 (2019).
13. Panasiti, M. S. *et al.* Thermal signatures of voluntary deception in ecological conditions. *Scientific reports* **6,** 1–10 (2016).
14. Or, C. K. & Duffy, V. G. Development of a facial skin temperature-based methodology for non-intrusive mental workload measurement. *Occupational Ergonomics* **7,** 83–94 (2007).
15. Shastri, D., Papadakis, M., Tsiamyrtzis, P., Bass, B. & Pavlidis, I. Perinasal imaging of physiological stress and its affective potential. *IEEE Transactions on Affective Computing* **3,** 366–378 (2012).
16. Goldberger, A. L. & West, B. J. Fractals in physiology and medicine. *The Yale journal of biology and medicine* **60,** 421 (1987).

17. Vuksanović, V., Sheppard, L. W. & Stefanovska, A. Nonlinear relationship between level of blood flow and skin temperature for different dynamics of temperature change. *Biophysical journal* **94,** L78–L80 (2008).
18. Kitney, R. An analysis of the nonlinear behaviour of the human thermal vasomotor control system. *Journal of Theoretical Biology* **52,** 231–248 (1975).
19. Di Credico, A. *et al.* Estimation of Heart Rate Variability Parameters by Machine Learning Approaches Applied to Facial Infrared Thermal Imaging. *Frontiers in Cardiovascular Medicine* **9** (2022).
20. Sugihara, G. *et al.* Detecting causality in complex ecosystems. *science* **338,** 496–500 (2012).
21. Nardelli, M., Vanello, N., Galperti, G., Greco, A. & Scilingo, E. P. Assessing the quality of heart rate variability estimated from wrist and finger ppg: A novel approach based on cross-mapping method. *Sensors* **20,** 3156 (2020).
22. Nardelli, M., Greco, A., Vanello, N. & Scilingo, E. P. *Reliability of Pulse Rate Variability in Elderly Men and Women: An Application of Cross-Mapping Approach* in *2021 43rd Annual International Conference of the IEEE Engineering in Medicine & Biology Society (EMBC)* (2021), 492–495.
23. Stroop, J. R. Studies of interference in serial verbal reactions. *Journal of experimental psychology* **18,** 643 (1935).
24. Nirkin, Y., Masi, I., Tuan, A. T., Hassner, T. & Medioni, G. *On face segmentation, face swapping, and face perception* in *2018 13th IEEE International Conference on Automatic Face & Gesture Recognition (FG 2018)* (2018), 98–105.
25. Gioia, F., Pascali, M. A., Greco, A., Colantonio, S. & Scilingo, E. P. *Discriminating Stress From Cognitive Load Using Contactless Thermal Imaging Devices* in *2021 43rd Annual International Conference of the IEEE Engineering in Medicine & Biology Society (EMBC)* (2021), 608–611.
26. Tarvainen, M. P., Niskanen, J.-P., Lipponen, J. A., Ranta-Aho, P. O. & Karjalainen, P. A. Kubios HRV–heart rate variability analysis software. *Computer methods and programs in biomedicine* **113,** 210–220 (2014).
27. Kennel, M. B., Brown, R. & Abarbanel, H. D. Determining embedding dimension for phase-space reconstruction using a geometrical construction. *Physical review A* **45,** 3403 (1992).
28. Benjamini, Y., Krieger, A. M. & Yekutieli, D. Adaptive linear step-up procedures that control the false discovery rate. *Biometrika* **93,** 491–507 (2006).